Supporting Information

Three-dimensionally filler thermal network structured GnPs&MWCNTs@PBO/PEEK composites integrating high thermal conductivity and electromagnetically shielding

Yageng Bai [a], Hongxia Qian [b], Xueling Cao [c], Fengyu Wen [a], Yashu He [a], Jierun Ma [a], Lin Cheng [a], Yifan Wang [a], Haoyuan Tan [a], Yuxuan Gu [a], Pengbo Lian [a], Rui Chen [d,], Jianxin Mu [a,]**

[a] *Key Laboratory of High Performance Plastics, Ministry of Education, National & Local Joint Engineering Laboratory for Synthesis Technology of High Performance Polymer, College of Chemistry, Jilin University, Changchun 130012, P. R. China*

[b] *Siping Experimental Middle School, Siping 136000, P. R. China*

[c] *College of Science, Qiongtai Normal University, Haikou 571100, P. R. China*

[d] *Light Industry and Chemical Engineering, Guangdong University of Technology, Canton 510006, P. R. China*

* Corresponding author:

Prof. Jianxin Mu

E-mail: Jianxin_mu@jlu.edu.cn

Dr. Rui Chen

E-mail: jrchen1136@163.com

Table of Contents

Results and discussion supplementary

SEM images in **Fig. S1(a, b)** depicts the surface of GnPs&MWCNTs@PBO composites with two filler contents. During the formation of the thermally conductive network in the GnPs&MWCNTs@PBO composites, the PBO fiber balls is believed to play a role in "volume exclusion". This effectively increases the local concentration of carbon nanofillers in the microscopic regions, creating more pathways for heat conduction. In addition, the dense stacking structure of the carbon nanofillers significantly enhances the interfacial interactions between the nanofillers, directly reducing the interfacial thermal resistance and improving phonon transport. Additionally, **Fig. S1(c, d)** illustrates the formation of a continuous thermally conductive network structure by the deposition of carbon nanofillers on the surface of PBO fiber balls. The strong interfacial interaction between carbon nanofillers and PBO fiber balls promotes uniform filler deposition through π-π stacking. The inclusion of PBO increases the contact area between different carbon nanomaterials, thereby enhancing the number of pathways for thermal conduction. **Fig. S1(e, f)** shows SEM images of the cryo-fractured surfaces of GnPs&MWCNTs@PBO/PEEK composites with a filler content of 19.31 vol%. The blue dashed lines depict the tendency of MWCNTs to align vertically. It is evident that, while a small fraction of MWCNTs may align horizontally due to hot-pressing pressure, the majority of these 1D structures prefer vertical alignment, forming continuous pathways for thermal conduction. This alignment significantly enhances the through-plane thermal conductivity of GnPs&MWCNTs@PBO/PEEK composites.

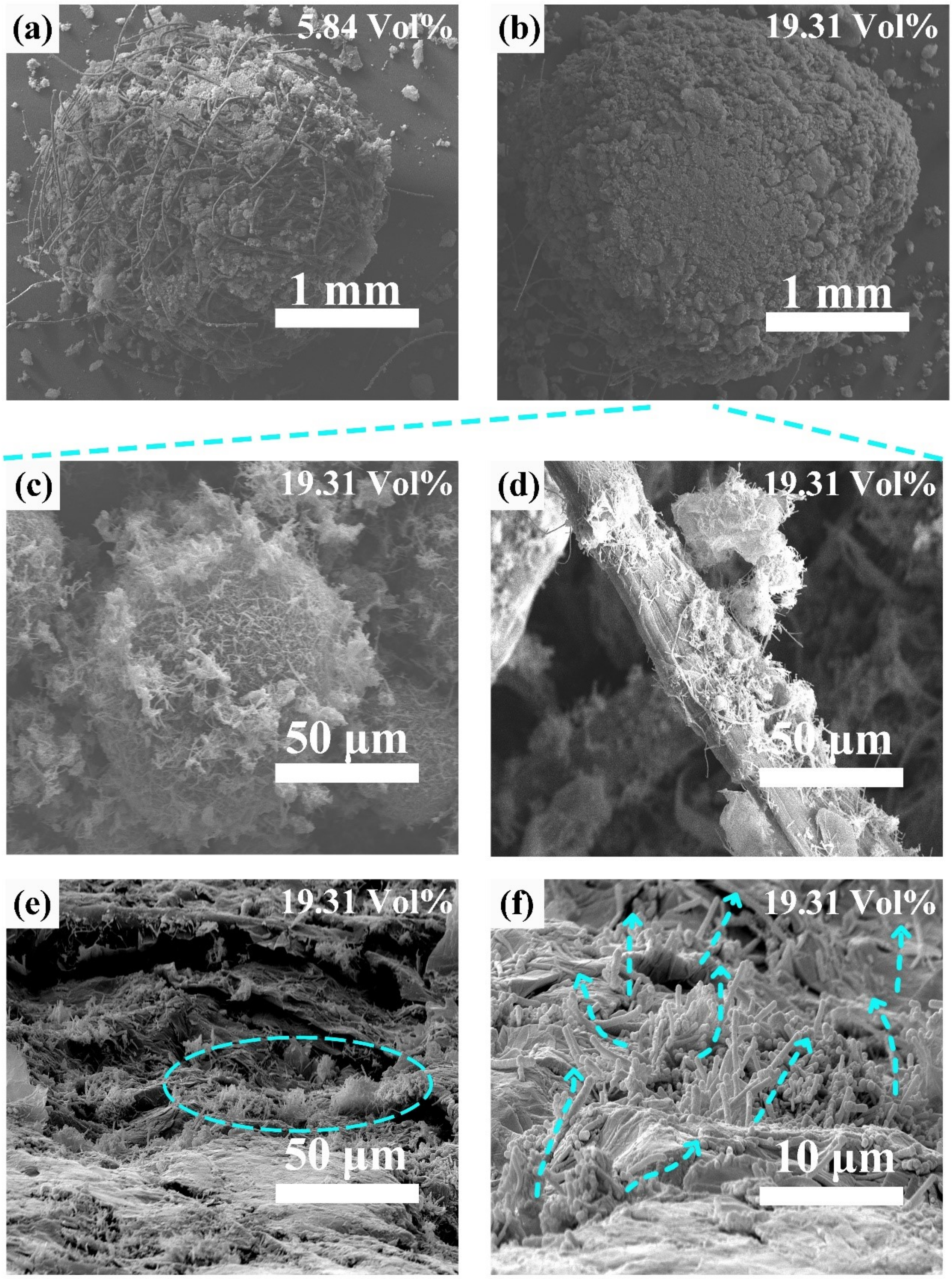

Fig. S1 (a, b) GnPs&MWCNTs@PBO composites with two filler contents; (c) and (d) represent the local enlarged images of (b); (e, f) SEM images of the cryo-fractured surface of GnPs&MWCNTs@PBO/PEEK composites.

Composites containing two or multiple fillers often exhibit a synergistic enhancement in thermal conductivity. At a microscopic level, the "nano-microbridge" effect created by varied fillers results in the formation of numerous crossing points or contact lines, increasing the contact area of the fillers while simultaneously reducing the contact area of the polymer-fillers. This reduction in interface thermal resistance significantly enhances heat transfer efficiency. Thus, to attain an optimal ratio of GnPs and MWCNTs in the composites, the GnPs&MWCNTs@PBO/PEEK composites were fabricated using various ratios of carbon fillers, followed by the comparison of their thermal conductivity. As indicated in **Table S1**, composites with a filler ratio of 7:3 (GnPs : MWCNTs) demonstrated optimal thermal conductivity within the specified physical parameters of the fillers. Therefore, this specific ratio was selected for the subsequent experiments.

Table S1 TC values of the composites prepared by using various proportions of the fillers (with a total filler content of 19.31 vol%).

Ratio of (GnPs and MWCNTs）	TC-Through Plane ($W{\cdot}m^{-1}K^{-1}$)	TC-In Plane ($W{\cdot}m^{-1}K^{-1}$)
8：2	2.69	20.25
7：3	3.19	22.17
6：4	2.84	19.63
5：5	2.58	16.34

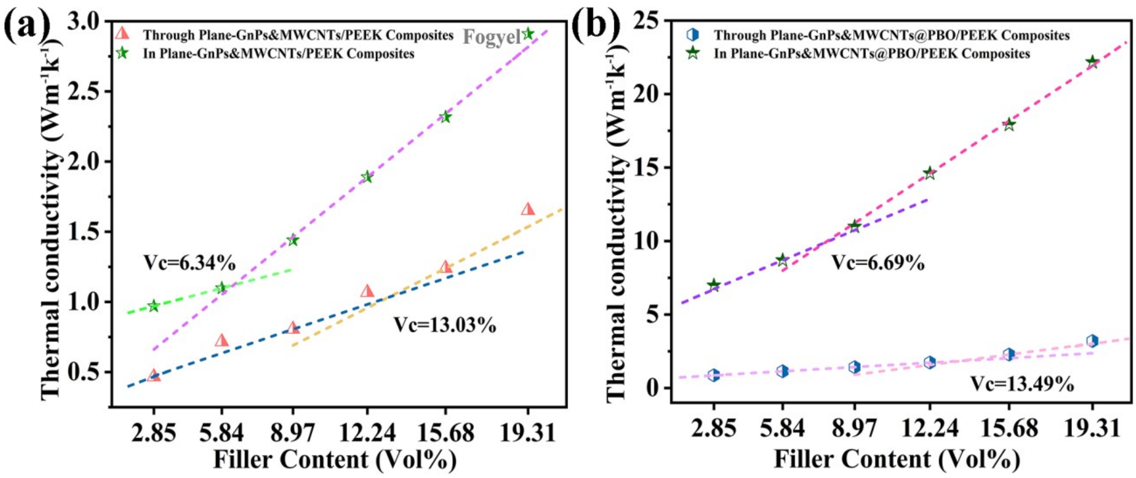

Fig. S2 (a, b) Foygel model-based Vc (through and in-planes) fitting curves of GnPs&MWCNTs@PBO/PEEK and randomly blended control composites.

Table S2 Parameters related to Rc fitting.

Sample	V_C(Vol%)	β	K_0	R_C(KW^{-1})	R_{it} ($m^2 \cdot WK^{-1}$)
In plane-GnPs&MWCNTs@PBO/PEEK	6.69	0.47	47.0	7.94×10^3	4.58×10^{-8}
Through plane-GnPs&MWCNTs@PBO/PEEK	13.49	0.37	8.2	1.74×10^4	2.09×10^{-8}
In plane-GnPs&MWCNTs/PEEK	6.34	0.39	4.0	6.06×10^4	1.63×10^{-6}
Through plane-GnPs&MWCNTs/PEEK	13.03	0.48	6.6	6.16×10^4	1.60×10^{-6}

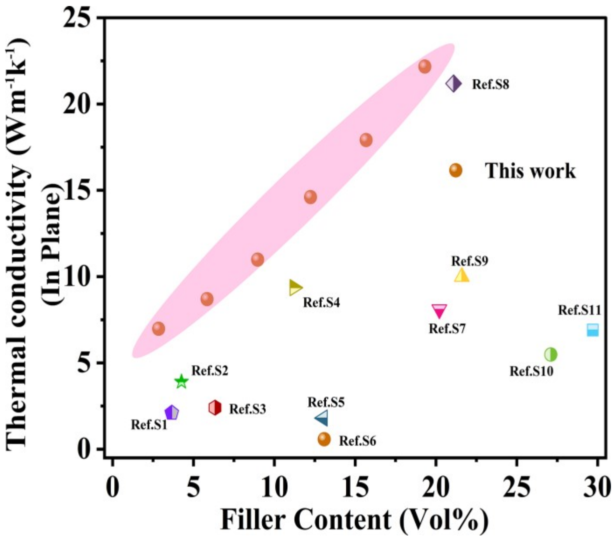

Fig. S3 Comparison of the TC values of GnPs&MWCNTs@PBO/PEEK composites and previously reported filled polymeric composites [1-11].

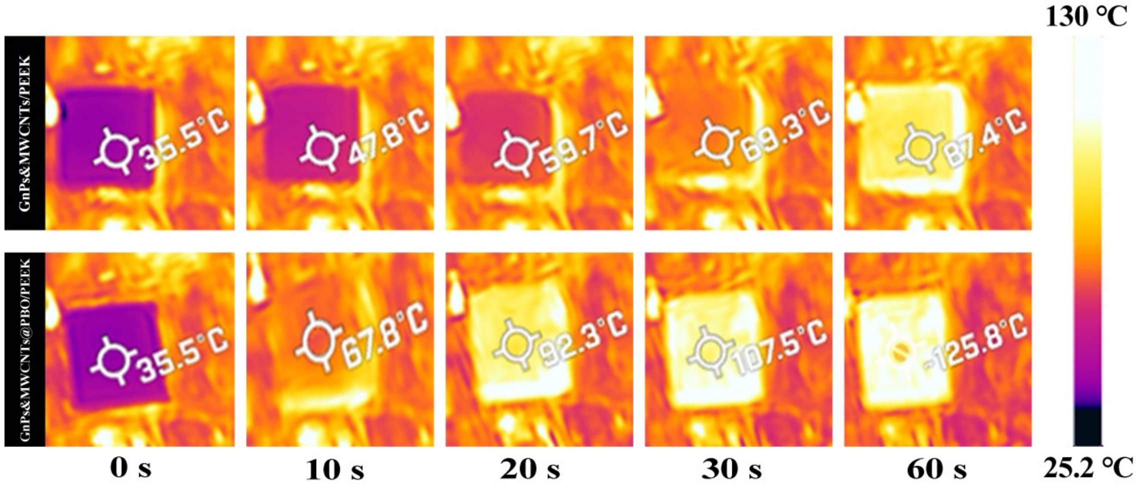

Fig. S4 Infrared thermal images of the contrast samples at various heating durations.

Simulation part

A 3D solid heat transfer model with a size of 1 mm × 1 mm × 1 mm was employed to facilitate the computational process. The GnPs&MWCNTs/PEEK and GnPs&MWCNTs@PBO/PEEK composites were determined to have respective in-plane thermal conductivities of 2.91 $W \cdot m^{-1}K^{-1}$ and 22.17 $W \cdot m^{-1}K^{-1}$. A boundary heat source of 100 °C was applied to the left side of the model using the solid heat transfer module. All other external boundaries were set as heat-insulated, with an initial temperature of 20 °C.

The concentration of PBO used for modification significantly influences the thermal conductivity of the PEEK matrices, as shown in Fig. S5. The results show a marked enhancement in the thermal conductivity of PBO@PEEK composites compared to pure PEEK. As shown in Fig. S5, the composites attained optimal thermal conductivity at a filler ratio of 7:3 (PBO: PEEK), aligning with the specific physical parameters of the fillers. The corresponding PBO to PEEK ratio was chosen for further experiments. As illustrated in **Fig. S5b**, the thermal conductivity of GnPs&MWCNTs@PBO/PEEK composites is demonstrably higher than that of GnPs/MWCNTs@PBO/PEEK composites at a filler content of 19.31 vol%. Bridging 1D MWCNTs with 2D GnPs can significantly enhance the through-plane thermal conductivity of nanocomposites. The approach effectively enhances the interfacial contact area between fillers, thereby significantly improving the overall thermal conductivity of GnPs&MWCNTs@PBO/PEEK composites.

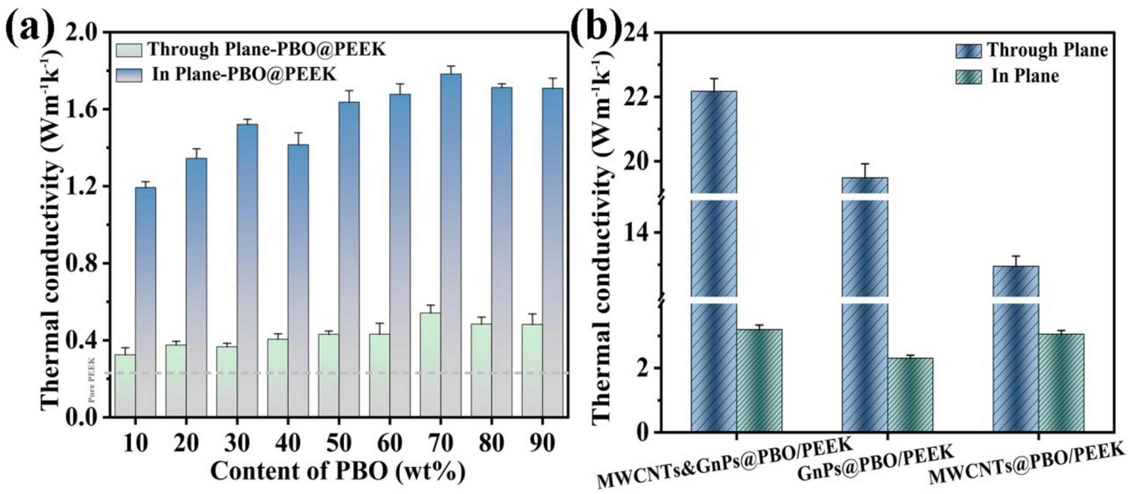

Fig. S5 (a) Thermal conductivity data of GnPs&MWCNTs@PBO/PEEK composites with different PBO concentrations; (b) Comparison of thermal conductivity of three composites at a filler content of 19.31 vol%.

Equation part

The conductive percolation threshold of the composites was simulated according to the classical Kirkpatrick-Zallen **Eq. (S1)**, where σ and σ_f denote the conductivities of the composites and fillers, respectively; t denotes the number of dimensions associated with the conductive network within the composites; and Φ and Φ_C represent the total volume fraction and critical volume fraction of the fillers for electrical percolation.

$$\log \sigma = \log \sigma_f + t\log\left(\frac{\emptyset - \emptyset_c}{1 - \emptyset_c}\right) \quad \text{……………………..…(S1)}$$

Table S3 Thermal characteristics of GnPs&MWCNTs@PBO/PEEK composites.

Samples	Weight loss temperature(°C)		T_{HRI}*(°C)
	T_5	T_{30}	
PEEK	562	589	283
2.85 Vol%	597	743	335
5.84 Vol%	595	753	338
8.97 Vol%	590	774	343
12.24 Vol%	596	781	346
15.68 Vol%	586	793	348
19.31 Vol%	589		

"Heat-resistance index (T_{HRI})" is an effective parameter to assess the thermal stability of the composites. Heat-resistance index (T_{HRI}) was computed using the **Eq. (S2)**:

$$T_{HRI} = 0.49*[T_5 + 0.6*(T_{30} - T_5)] \quad \text{(S2)}$$

Where, T_5 and T_{30} were the decomposition temperature corresponding to 5% and 30% weight loss, respectively.

Reference

[1] Y. Shang, D. Zhang, M. An and Z. Li, *Materials*, 2022, **15**, 5380-5392.

[2] J. Gao, G. Han, J. Song, C. He, J. Hu, W. Wang, Y. Feng and C. Liu, *Mater. Today Phys.*, 2022, **27**, 100811-100821.

[3] Z. Jiang, B. Jiang, B. Yang, X. Liu, Y. Yang, C. Zhang, Y. Shang and H. Zhang, *Adv. Mater. Interfaces*, 2023, **10**, 2202508-2202518.

[4] T. Gu, D. Sun, X. Xie, X. Qi, J. Yang, C. Zhao, Y. Lei and Y. Wang, *Compos. Sci. Technol.*, 2022, **230**, 109757-109769.

[5] S. Chauhan, P. N. Mohan, K. C. J. Raju, S. Ghotia, N. Dwivedi, C. Dhand, S. Singh and P. Kumar, *Colloids Surf. A*, 2023, **673**, 131811-131820.

[6] C. Zhang, K. Deng, X. Li, K. Fu and C. Ni, *ACS Appl. Nano Mater.*, 2023 **6**, 13400-13408.

[7] J.-U. Jang, H. E. Nam, S. O. So, H. Lee, G. S. Kim, S. Y. Kim and S. H. Kim, *Polymers*, 2022, **14**, 323-333.

[8] Z. Ali, X. Kong, M. Li, X. Hou, L. Li, Y. Qin, G. Song, X. Wei, S. Zhao, T. Cai, W. Dai, C. Lin, N. Jiang and J. Yu, *Fibers Polym.*, 2021, **23**, 463-470.

[9] X. Wang, H. Lu, C. Feng, H. Ni and J. Chen, *Plast., Rubber Compos.*, 2020, **49**, 196-203.

[10] Y. Sun, M. Zhang, Y. Zhang, J. Luan, H. Dang, D. Jiang and Y. Yang, *Compos. Commun.*, 2021, **28**, 100909-100915.

[11] S. Yang, Z. Jin, C. Song, Z. Pu and B. Wen, *J. Mater. Sci.*, 2022, **57**, 1084-1097.